IEEE Transactions on Control Systems Technology, Available online 13 May 2024
DOI:10.1109/TCST.2024.3395722

Optimal Control of Race Car with Aerodynamic Slipstreaming Effect

Xuze Liu, Abbas Fotouhi, *Senior Member, IEEE*, Marco Cecotti, Daniel Auger, *Senior Member, IEEE*

***Abstract*— This paper presents a new method to describe the aerodynamics slipstreaming effect on the downstream car. This new approach can be implemented in lap time simulations and used to study the optimal trajectory of a downstream car operating in the wake of an upstream car. Two different scenarios are investigated using this method. In the energy-saving scenario for electric racing cars, the result shows the optimal strategy varies depending on the upstream car's pace and the initial gap between the two cars. Chasing to stay in the wake is less effective when the initial gap is relatively big. In the overtaking scenario on an oval track, it is shown that the wake of the upstream car benefits the downstream car's acceleration but meanwhile reduces the lateral performance limit of the downstream car due to downforce loss. In order to maintain a competitive performance, it is essential for the downstream car to choose an alternative racing line to drive outside the wake when braking and passing through a corner.**

***Index Terms*— Optimal control, Lap time simulation, Aerodynamic slipstreaming.**

I. Introduction

In recent years, aerodynamics has become increasingly important in race car design and optimizations. Engineers spend a big amount of effort on optimizing the aerodynamic performance to achieve a faster lap time. While most of the studies focus on a single-car analysis, in real-life races, the aerodynamic interactions between cars also have a big impact on vehicle performance. The wake of a leading car normally creates a low-pressure region behind it which affects the airflow and therefore the aerodynamic forces on the following car. This usually leads to a loss of drag and downforce on the following car, i.e. slipstreaming hence could potentially result in a net speed advantage or energy saving, both of which could be beneficial. However, such a region of low pressure is usually very small and recovers very quickly. Therefore, to make the best of this slipstreaming effect, good trajectory planning and execution are required.

In motorsport, lap time simulations (LTS) are the most commonly used tool to find out the maximum achievable performance of a race car on a specific track. In the literature, dynamic programming [1] and convex optimizations [2] are often used for problems with simplified systems and fixed racing lines. When high-fidelity system dynamics are used and the racing line needs to be optimized simultaneously, the optimal control technique proves to be the most efficient approach. Such a technique can be used not only as a tool for simulation but also for optimizations. For instance, the effect of a limited-slip differential(LSD) on optimal trajectory on different road frictions can be studied [3]. In the meantime, the LSD characteristics can be optimized by formulating an optimal control problem to find the best setup for the maximum performance of a vehicle [4]. The optimal control technique is very efficient in solving a constrained problem. Therefore, it can be used to study the best trajectory while respecting various constraints. For top-level race cars, tyre usage and powertrain energy management are crucial for vehicle performance. In [5], by introducing the temperature effect on tyre performance and formulating the tyre wear into an integral constraint, the optimal tyre usage strategy is investigated. The hybrid energy management of a modern Formula One (F1) powertrain is modelled in [6] and the optimal energy flow between different components, ie. Internal combustion energy, motor-generator units (MGU), is studied. By further simplifying the model to improve computational efficiency, Soren, et al. [7] implemented such optimization technique in real time to manage the powertrain hybrid system. With full-electric motorsport becoming more and more popular in recent years, more literature has started to focus on the battery energy management of race cars[8]. Liu et al. modelled a Formula E (FE) car integrated with a battery thermal dynamics model. It was concluded that the "lifting and coasting" techniques were the most efficient method to make the best of a limited amount of energy to achieve the fastest possible lap times. The optimal control technique in general is able to accommodate more complex systems. In [12] and [13], the track is modelled as a ribbon with 3D features such as elevation and banking. Furthermore, Masouleh et al. [13] improved the vehicle model fidelity by introducing a multilink suspension system and interactions between aerodynamics and suspension. Such optimal control problem formulation allows more features to be optimized in a single simulation instance instead of ordinary exhaustive searches.

In the literature, the LTS is formulated featuring only one car and none has analyzed dual-car scenarios. However, the aerodynamic characteristics of a race car operating in a wake have been analyzed in several studies. Wilson, et al. [14] studied the wake structure and the aerodynamic characteristics of a single wing operating in the wake. It is pointed out that the wake structure is dominated by a trailing vortex pair coupled

All authors are with the Advanced Vehicle Engineering Centre, School of Aerospace, Transport and Manufacturing, Cranfield University, MK43 0AL, UK (e-mails: xuze.liu@cranfield.ac.uk; a.fotouhi@cranfield.ac.uk; m.cecotti@cranfield.ac.uk; d.j.auger@cranfield.ac.uk).

© 2024 IEEE. Personal use of this material is permitted. Permission from IEEE must be obtained for all other uses, in any current or future media, including reprinting/republishing this material for advertising or promotional purposes, creating new collective works, for resale or redistribution to servers or lists, or reuse of any copyrighted component of this work in other works.

with intense turbulence which has a manifest effect on the following car. The wake influence on the isolated wing reduces rapidly with increasing inter-vehicle spacing. Similarly in [15], it is shown in detail how the pressure distribution of a single wing element is affected by the wake. On a full-vehicle level, Gan, et al [15] investigated the drag characteristics of a NASCAR race car operating in the wake using computational fluid dynamics (CFD) simulations. The result shows slipstreaming is most beneficial to downstream cars at short inter-vehicle spacings and this drafting is potentially creating overtaking opportunities for the downstream. In [17] and [18], high-fidelity Formula One (F1) vehicle models are used in CFD simulations to investigate more realistic wake effects on a modern race car. The studies found that both the aerodynamic downforce and the drag of the downstream car reduce and these reductions are greater with closer proximity. Additionally, the aerodynamic balance of the downstream also changes in the presence of the wake which fundamentally changes the pressure distribution of the downstream car.

While there is clear evidence that the aerodynamic characteristics (lift coefficient C_l and drag coefficient C_d) can be affected by an upstream car, none has investigated such effect in the LTSs. The raw results from the CFD studies cannot be easily introduced into LTSs. The changes in C_l and C_d of the downstream car are presented as a function of relative positions and velocity. One of the main assumptions of these CFD simulations is that the velocities of both vehicles are identical and constant (due to stationary vehicles and free-stream settings in CFD). This is very different from real-life events where technically two cars rarely have identical speeds at the same time. The biggest issue in formulating the slipstream effect as a simple interpolation is to choose the upstream or downstream vehicle velocity as the velocity input for interpolation. Unfortunately, in this case, neither would make perfect sense because two cars are at different positions on the track (no matter how far or close they are) hence the speeds are hardly identical. Therefore, a new approach is needed to describe the slipstreaming effect so that it can be used in lap time simulations to investigate the vehicle performance in the presence of another car.

In this paper, we investigate two of the most popular scenarios where slipstreaming might be beneficial: Formula E (FE), as an example of a full-electric racing series, and Indy 500, as an example of high-speed racing with long straights and minimal performance difference. First, in FE, energy management is one of the most crucial elements in race strategy development. A driver can potentially save energy by slipstreaming behind another car. This could accumulate through laps and in the later stages of a race would lead to an energy advantage which could be used for overtaking. Second, overtaking in motorsport occurs when the chasing car has a net speed advantage over the leading car. In FE, this is relatively easier because all drivers need to lift and coast at high-speed sectors in order to save energy [9] which leaves a big margin from the vehicle's true dynamic limit. Therefore, to overtake an opponent, one only has to do less coasting (i.e. continue to accelerate) and speed advantage can be easily created although with additional energy cost. In contrast, in other racing series like the Indy 500 where energy/fuel efficiency isn't the top priority and vehicles have similar performances, apart from driver factors, slipstreaming might be one of the few options to create a speed advantage in order to make overtaking attempts. This paper is formulated into five sections. The problem background and research gap are introduced in section I. The track and vehicle model with slipstreaming effect are presented in section II. The formulation of an optimal control problem is shown in section III. Section IV demonstrates the results. Finally, conclusions are presented in section V.

II. Track and Vehicle Modelling

A. Track modelling

In this paper, the vehicle and the track models are created based on the curvilinear coordinate instead of using a Cartesian coordinate system. In such curvilinear coordinates, the track is described using a single piece of distance-based information, namely the curvature as shown in figure 1. This is more computationally efficient than the Cartesian coordinate system that uses x and y coordinates to describe the track.

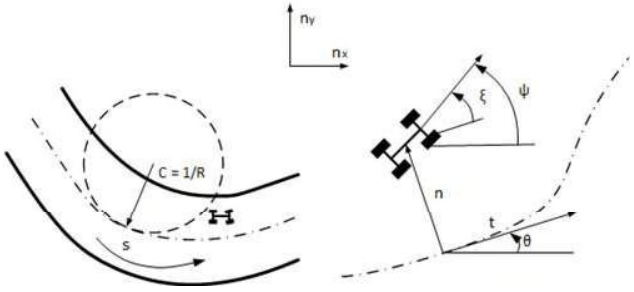


Fig. 1. Track curvilinear coordinates

As a consequence, the car's position is described using *s* which indicates how far the car has travelled along the track centreline, and *n* which is the distance of the vehicle mass centre from the centerline, taken perpendicularly to the centerline's tangent direction. In this way, the track limit can be more efficiently bounded in the optimal control problem by only limiting the bound for n. The positions of the car are treated as vehicle states whose derivatives can be calculated by:

$$\dot{s} = \frac{u\cos\xi - v\sin\xi}{1 - nC} \tag{1}$$

$$\dot{n} = u\sin\xi + v\cos\xi \tag{2}$$

where u and v are the longitudinal and lateral velocities of the vehicle. ξ describes the relationship between the vehicle heading direction and the track centerline tangent direction and is calculated by:

$$\dot{\xi} = \dot{\psi} - C\dot{s} \tag{3}$$

in which $\dot{\psi}$=ω is the vehicle yaw rate and will be later used in vehicle modelling. In this paper, we use dot notation to note the time derivatives to separate them from the distance derivatives which are used in the problem formulation. In the OCP (optimal control problem), we assume the travelled distance *s* is monotonically increasing. And because overtaking is a maneuver directly related to positions, in this study, s is used as

the independent variable instead of time. To differentiate the problem states in the distance domain from the time domain, the following conversion is implemented:

$$ds = \frac{ds}{dt}dt = \frac{u\cos\xi - v\sin\xi}{1-nC}dt \quad (4)$$

we define S_f representing the reciprocal of the velocity of the vehicle along the track centerline as:

$$S_f = (\frac{ds}{dt})^{-1} = \frac{1-nC}{u\cos\xi - v\sin\xi} \quad (5)$$

Therefore, we can calculate the lateral position of the vehicle n and angle ξ using:

$$\frac{dn}{ds} = (u\sin\xi + v\cos\xi)\cdot S_f \quad (6)$$

$$\frac{d\xi}{ds} = S_f\omega - C \quad (7)$$

It should be noted that in this paper, the sign conventions follow the rules that positive values of ω and C denote the angular change anti-clockwise. Positive n and v denote travel to the left-hand side.

B. Vehicle modelling

In this paper, the vehicle is modeled as a planar model with 7 degrees of freedom including longitudinal, lateral, and yaw motions with 4 wheel rotations. In addition to the conventional drive torques on the rear axle and brake torques at all four wheels, the front wheels are also controlled by the steering input and the rear wheels are affected by a limited-slip differential (LSD) modelled on the rear axle. Aerodynamics and load transfer effects are both accounted for. We model the car in two slightly different ways to suit the two different investigated scenarios. For the full-electric car, drive and regenerative brake torques are applied on the rear wheels and the mechanical brake is applied on the front wheel. For Indy-like scenarios, the regenerative brake on the rear axle will be replaced by the normal mechanical brake hence energy consumption will not be accounted for.

.

1) Body dynamics

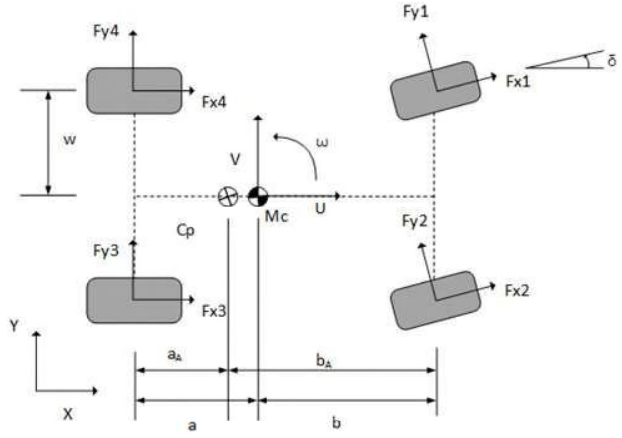


Fig. 2. 7 DOF Vehicle model.

The longitudinal, lateral and yaw motions of the body illustrated in figure 2 can be calculated using the following equations:

$$M\frac{d}{dt}u(t) = M\omega v + F_x \quad (8)$$

$$M\frac{d}{dt}v(t) = -M\omega u + F_y \quad (9)$$

$$I_z\frac{d}{dt}\omega(t) = a\cdot\left(\cos\delta\cdot(F_{y1}+F_{y2}) + \sin\delta\cdot(F_{x1}+F_{x2})\right) - w\cdot\left(\sin\delta F_{y2} - \cos\delta F_{x2}\right) + wF_{x3} - w\cdot\left(\cos\delta F_{x1} - \sin\delta F_{y1}\right) - w\cdot F_{x1} - b\cdot(F_{y3}+F_{y4}) \quad (10)$$

The descriptions of the symbols and numerical values are presented in table 1.

TABLE I
SYMBOLS AND DESCRIPTIONS

Symbol	Description	Value
M	Vehicle mass	900kg
I_z	Moment of inertia about the z-axis	450kgm2
δ	Front wheel steering angle	Input
w	Half track width	0.775m
a	Distance from the vehicle mass center to the rear axle	1.24m
b	Distance from the vehicle mass center to the front axle	1.86

Each tyre generates longitudinal and lateral forces, namely F_{xi} and F_{yi} respectively. The subscript i (i=1,2,3,4) denotes the tyre on the front left, front right, rear right and rear left corner. Accounting for the slip angles of the tyre, the total longitudinal and lateral forces F_x and F_y acting on the vehicle, are calculated by

$$F_x = \cos\delta\cdot(F_{x1}+F_{x2}) - \sin\delta\cdot\left(F_{y1}+F_{y2}\right) + (F_{x3}+F_{x4}) - F_{ax}$$

$$F_y = \cos\delta\cdot\left(F_{y1}+F_{y2}\right) + \sin\delta\cdot(F_{x1}+F_{x2}) + \left(F_{y3}+F_{y4}\right)$$

where F_{ax} is the longitudinal aerodynamic load on the car which will be defined in the next section.

2) Wheel dynamics and tyre normal loads

As aforementioned, each wheel contributes one DOF of rotation. These motions can be described based on the torques applied on the rotation dynamics using the following equations:

$$J_w\dot{\omega}_1 = k_bT_{brake} - F_{x1}R \quad (11)$$

$$J_w\dot{\omega}_2 = k_bT_{brake} - F_{x2}R \quad (12)$$

$$J_w\dot{\omega}_3 = T_{drive} + (1-k_b)T_{brake} - T_{diff_r} - F_{x3}R \quad (13)$$

$$J_w\dot{\omega}_4 = T_{drive} + (1-k_b)T_{brake} + T_{diff_r} - F_{x4}R \quad (14)$$

In which J_w is the wheel rotational inertia, k_b is the brake bias to the front, T_{drive} and T_{brake} are drive torque from the motor brake torque generated by the calliper or the motor regeneration, R is the tyre radius.

The T_{diff_r} is the LSD torque transferred from the faster-rotating wheel to the slower wheel. This torque is given by:

$$T_{diff} = 0.5k_d\cdot(\omega_3 - \omega_4) \quad (15)$$

where $\omega_3 - \omega_4$ is the difference between the rear left and right wheel angular on the rear axle and k_d is a constant rotational damping coefficient of the LSD.

In this paper, an empirical tyre model [34] is used for the tyre force calculations. This model uses linearized interpolation [35] to describe the change of peak values of longitudinal and lateral friction coefficient due to normal load variations. Model detail

is shown in appendix A.

To satisfy the vehicle motion equations, the normal forces acting on the tyres must respect the balancing equations as follows.

In the vertical direction:

$$F_{z1} + F_{z2} + F_{z3} + F_{z4} - Mg - F_{az} = 0 \quad (16)$$

Where F_{zi} are the tyre normal forces on each tyre. g is the acceleration due to gravity and F_{az} is the aerodynamic vertical load on the car.

For the moment around the x-axis and y-axis (illustrated in figure 2) of the car, the forces must satisfy:

$$w \cdot (F_{z4} - F_{z3}) + w \cdot (F_{z1} - F_{z2}) + hF_y = 0 \quad (17)$$

$$b \cdot (F_{z3} + F_{z4}) - a \cdot (F_{z1} + F_{z2}) - hF_x - (a_A - a)F_{az} = 0 \quad (18)$$

In which h is the height of the vehicle mass centre to the ground.

To ensure the vehicle dynamics is fully determined with a unique solution for the four normal forces, a fourth balancing equation is introduced with a lateral load transfer bias parameter D which describes the lateral load transfer distribution between the front and rear axle:

$$D \cdot (F_{z2} + F_{z3} - F_{z1} - F_{z4}) - F_{z2} + F_{z1} = 0 \quad (19)$$

The aero loads F_{az} and F_{ax} are given by:

$$F_{az} = 0.5C_l \cdot \rho_a \cdot A \cdot u^2 \quad (20)$$

$$F_{ax} = 0.5C_d \cdot \rho_a \cdot A \cdot u^2 \quad (21)$$

In which ρ_a is the air density and A is the frontal area of the car. C_d and C_l are the aerodynamic coefficients of drag and lift. In this paper, we formulate these two coefficients as functions. This is shown in the next section.

3) Slipstreaming effect

As pointed out in [17], the wake of a race car is dominated by a large vortex pair coupled with high turbulence intensity. From the energy point of view, while a race car is driving through the air, part of its kinetic energy is transferred to the air hence increasing the air's dynamic pressure. This lowers the static pressure in its trailing region which affects the downstream car that passes through it. Previous studies [16][17][18] demonstrate the change in aerodynamic characteristics of the downstream car as a function of relative spacing(longitudinal and lateral) between the two vehicles and one of the shared conclusions is that this effect is weaker with larger spacing. This can be interpreted in an alternative way by introducing a time element. The upstream car initializes a lateral low-pressure distribution across the width of the track at a longitudinal track position immediately after it passes. This high air kinetic energy then starts to dissipate meanwhile the static pressure in that lateral section recovers. The spacing between the vehicles determines the time that the downstream car needs to travel to that section. Therefore, with small spacing, the static pressure recovers very little hence the downstream car is significantly affected and conversely, large spacing affects the downstream car less.

We first propose a normal-distribution-like formula to describe the initial aerodynamic performance loss caused by the aforementioned initial lateral low-pressure distribution.

$$P_{loss,iniC} = \xi_C \cdot u_{US}^2 \cdot e^{\frac{-\Delta n^2}{\sigma_C}} \quad (22)$$

where u_{US} is the upstream car velocity, Δn is the relative lateral position of the downstream car to the upstream car, ξ_C is a scaler and σ_C is a distribution coefficient. The $P_{loss,iniC}$ quantifies the initial performance loss at time zero. In this paper, the downforce loss and drag loss share the same formulation but parameterized separately when used in eq. 23-25. The parameters used in the paper are listed in appendix C.

This initial performance loss will weaken with time. This weakening effect is described using the following equation.

$$P_{loss,C}(\Delta t) = P_{loss,iniC} \cdot \gamma_C \cdot arctan(\frac{1}{e^{k_C \cdot \Delta t}}) \quad (23)$$

where Δt is the time gap between the upstream and downstream car passing through a certain longitudinal position. The γ_C and k_C are scaling factors. It should be noted that ξ_C, and σ_C in equations (22) are coefficient specific that each has two values for lift and drag respectively. The aerodynamic characteristics of the downstream car can be calculated using:

$$C_{d_{DS}} = (1 - P_{loss,Cd}(\Delta t)) \cdot C_d \quad (24)$$

$$C_{l_{DS}} = (1 - P_{loss,Cl}(\Delta t)) \cdot C_l \quad (25)$$

where C_d and C_l are the vehicle's default coefficients in the freestream. In this study, we use the default aerodynamic performance in [9] and fit the equation based on the CFD simulation results from [17]. Figure 3 below shows an example of aerodynamic performance loss distribution over time and track lateral position at velocity of 60m/s.

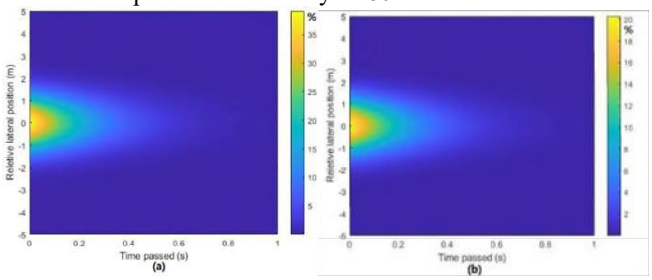


Fig. 3. Percentage of aerodynamic performance loss (a) Drag loss (b) Downforce loss.

Same as the conclusion in [17], the favourable reduction of drag disappears very quickly. In order to make the best of the slipstreaming effect, the downstream car needs to stay within a very short distance from the upstream car. Meanwhile, the downstream car also faces downforce loss which makes it difficult to stay close in the high-speed corners. The optimal trajectory solutions will be demonstrated in section IV.

III. Optimal Control Problem Formulation

The optimal control problem is formulated in order to solve the problem of minimizing the cost function in Bolza form, that is:

$$J = \emptyset(t_0, x(t_0), t_f, x(t_f), p) + \int_{t_0}^{t_f} l(t, x(t), u(t), p)dt \quad (26)$$

Which is subject to the constraints of

$$\begin{cases} \frac{dx}{dt} - f(t, x(t), u(t), p) = 0 \\ g(t, x(t), u(t), p) = 0 \\ h(t, x(t), u(t), p) \leq 0 \\ g_b(x(t_0), x(t_f), u(t_0), u(t_f), p) = 0 \end{cases} \quad (27)$$

where the first term in equation (26) is the Major (boundary) cost and the latter term is the Lagrange cost.

In this formulation, $p \in R^{n_p}$ is the constant parameter vector of n_p dimensions that can be optimised, $x(t) \in R^n$ and $u(t) \in R^m$ are the state and the control vector respectively. The system ODE dynamics such as eq. 1-3,8-14 are described in the vector $f(t, x(t), u(t), p) \in R^n$. Vector $g \in R^{n_g}$ and $g_b \in R^{n_{gb}}$ are the equality constraints and the boundary constraints such as eq.16-19. The inequality constraints including integral inequality constraints such as eq. 29 and path inequality constraints like eq. 30, 31, 35 and 36 are defined in $h \in R^{n_h}$.

In this section, we will present how the problem is formulated for the two scenarios aforementioned in section I and the essential parts such as upstream car trajectory and collision constraints.

A. Upstream car trajectory

Before formulating the dual-car scenarios, we first formulate a single car problem to generate a reference car (i.e. upstream car) trajectory. This trajectory will be used in the slipstreaming calculations where the information of the upstream car is needed.

In this study, two different track layouts are used for the two scenarios. For the full electric energy-saving scenario, the Marrakesh E-Prix track is used. For the Indy-like overtaking scenario, an oval track layout will be used. The layouts are shown in figure 6.

In top motorsport categories nowadays such as Formula One and Formula E, the total amount of propulsion energy is always limited by regulations. In many cases, drivers or engineers need to carefully manage such limited resource onboard in order to make the best end-of-race result out of it. For instance, one of the crucial decisions to make, in a FE race, is 'Energy Per Lap' (EPL) which indicates the target energy consumption during a single lap.

According to [9], the most common way to save energy while maintaining a competitive speed is through techniques referred to as lift and coasting (LaC). As a result of not fully deploying the energy, the energy consumption of such a lap is usually much lower than a flat-out lap during which energy saving is not considered. If not respecting the strategy target, teams or drivers might encounter a potentially flat battery when it gets close to the finish of the race.

An example of such LaC technique is shown in figure 4.

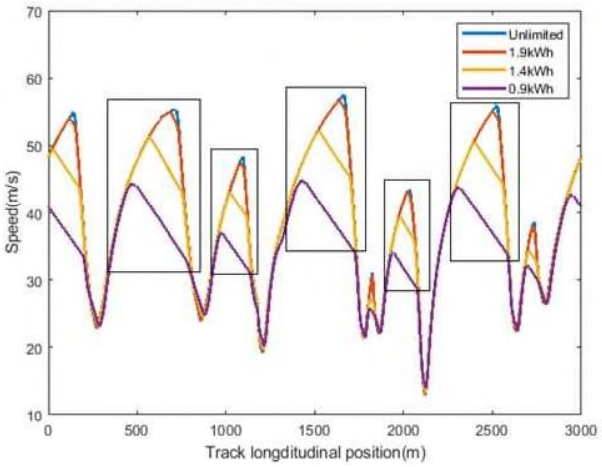


Fig. 4. Speed profiles using different energy per lap (EPL).

Effectively, the drivers need to lift their foot off the acceleration pedal and let the car coast using the remaining momentum with or without a certain amount of regenerative coasting torque. This technique is mostly seen before the end of a straight where the car reaches a high speed and starts to brake. As shown in figure 4, using such a technique would lead to a lower speed profile than the unlimited case in which energy saving is not considered. In this paper, we first generate a range of trajectories under different energy consumption constraints which will be used for investigation of how much energy can be saved when the upstream car is under different strategies. Such reference trajectories are generated by formulating a single car OCP of minimal time maneuver (MTM) with a boundary constraint of EPL, and based on the cost function of

$$J = \int_{s_0}^{s_t} Sf \, ds \quad (28)$$

where s_0 and s_t are the initial and terminal length of the track respectively. The energy constraint is added as

$$g_{bE} = \int_{s_0}^{s_t} (P_{power} \cdot Sf) ds \leq E_{epl} \quad (29)$$

in which E_{epl} is the upper limit of total energy consumption per lap, $P_{power} = P_{drive} + P_{regen}$ is the combination of propulsion and regeneration power given by:

$$P_{drive} = (T_{drive} + T_{diff_r})\omega_4 + (T_{drive} - T_{diff_r})\omega_3 \quad (30)$$

$$P_{regen} = ((1 - k_b)T_{brake} + T_{diff_r})\omega_4 + ((1 - k_b)T_{brake} - T_{diff_r})\omega_3 \quad (31)$$

In this scenario, P_{drive} will be given a boundary of 200kW which is the normal race mode setting in FE races.

For the slipstreaming overtaking scenario, the boundary of P_{drive} is raised to 400kW to replicate a similar performance of an Indy car. No energy-related constraints are applied assuming the upstream car isn't making any compromise in its lap so that the overtaking is all up to the downstream car. The cost function of this scenario is the same as equation (28) in the first scenario. This trajectory generation procedure of a single car is thoroughly explained in [9] thus, it is not detailed here. The reference trajectory provides the information in table 2, which will be used in the dual-car problem formulation.

TABLE II
Reference trajectory information

Information	Description
$t_{US}(s)$*	The time t_{US} of the upstream car travels through track position s
$s_{US}(t)$*	Longitudinal position s_{US} of the upstream car at time t
$u_{US}(s)$	The longitudinal speed u_{US} of the upstream car at track position s
$n_{US}(s)$	The lateral position n_{US} of the upstream car at track position s

* It should be noted that these two pieces of information are included for different purposes. $t_{US}(s)$ is used for slipstream effect calculations and $s_{US}(t)$ is used for the collision constraint calculation demonstrated in the next section.

B. Collision constraint

One of the most important principles when racing on track is not to collide with other competitors. In this trajectory optimization problem, to mimic real-life rules, we strictly forbid the downstream car to not collide with the upstream car. In the literature where trajectory planning is studied for autonomous vehicles, the collision avoidance among multiple vehicles is usually formulated as a soft constraint in which the collision avoidance cost is minimized at each step within the optimization horizon [21]. In motorsport, lap time or energy is usually the main cost to minimize. Adding a collision avoidance cost in the Lagrange cost will compromise the optimality of the solution of either time or energy. Therefore, in this study, we account for collision as a hard constraint outside the cost function.

There are two major assumptions in this constraint formulation. Firstly, the upstream car trajectory is assumed to be fixed, ie. not changing actively, in every single case. This mainly accounts for the fact that in real-life motorsport no leading driver would give up the optimal trajectory to initially avoid a collision when an opponent is trying to approach or overtake. This is different from cooperative autonomous trajectory planning [22] where the trajectories of each car are optimized simultaneously and cooperatively to avoid a collision. Additionally, a defensive maneuver from the upstream car is not considered which would lead to a completely different gaming problem. If the downstream car is about to pass the upstream car, we introduce a second assumption that the overtaking car is allowed to overlap the upstream car trajectory once it gains the longitudinal position advantage greater than zero. This 'collision neglecting' assumption is mainly accounting for the priority on the track. Once the downstream car passes the abreast position with the upstream car, the priority of maneuver is transferred to the overtaking car and the overtaken car then becomes responsible for collision avoidance. This is effectively similar to the concept of 'blocking' or 'defending' position in motorsport. Based on these two assumptions, the collision constraint used in this study is illustrated in Figure 5.

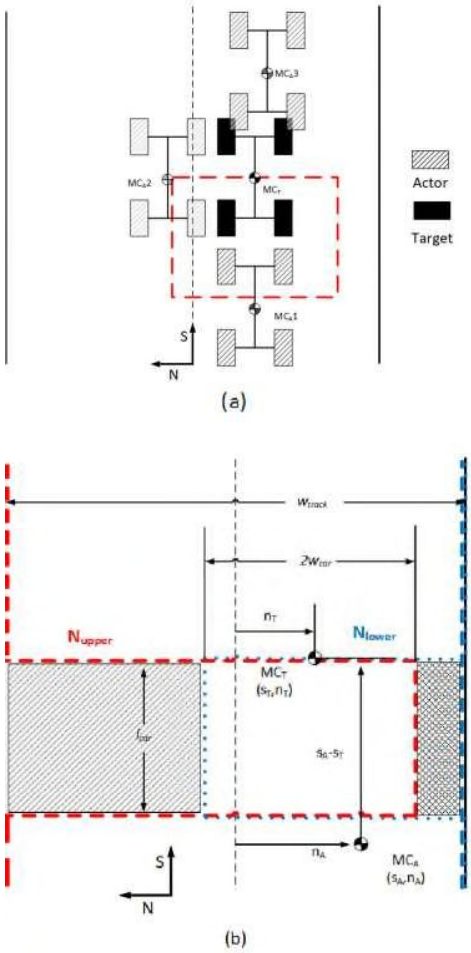


Fig. 5. Collision exclusive zone.

The majority of literature regarding collision avoidance uses quadratic distance (i.e. a circle) to model the collision exclusive zone [23]. In this study, the zone is described using a rectangular whose front edge starts from the centre of the upstream car. The rectangle has the same length and twice width as the car laterally symmetrical about the longitudinal car centreline. Such an approach would guarantee a precise description of the collision zone so that no track space is overlooked that might lead to potential overtaking opportunities. The collision constraint is formulated as follows:

$$\begin{cases} N_{upper} - n_{DS} > 0 \\ n_{DS} - N_{lower} > 0 \end{cases} \tag{32}$$

where the lateral boundaries N_{upper} and N_{lower} are given by:

$$N_{upper} = \begin{cases} 0.5w_{road} & if \;\; n_{US} > n_{DS} \\ 0.5w_{road} + (w_{car} + 0.5w_{road} - n_{DS}) \cdot \begin{pmatrix} H(s_{DS} - s_{US}) + \\ H(s_{DS} - s_{US} + l_{car}) \end{pmatrix} & if \;\; n_{US} \le n_{DS} \end{cases} \tag{33}$$

$$N_{lower} = \begin{cases} 0.5w_{road} - \\ (w_{car} + 0.5w_{road} + n_{DS}) \cdot \begin{pmatrix} H(s_{DS} - s_{US}) + \\ H(s_{DS} - s_{US} + l_{car}) \end{pmatrix} \\ \qquad\qquad if \;\; n_{US} > n_{DS} \\ 0.5w_{road} \qquad\qquad if \;\; n_{US} \leq n_{DS} \end{cases} \quad (34)$$

where s and n are respectively the longitudinal and lateral position of a car on the track in the curvilinear coordinate system. The upstream car and the downstream car are denoted by the subscripts US and DS respectively. w_{car} and l_{car} are the car width and length. w_{road} is the road width. The function H is the Heaviside step function.

Both upper bound N_{upper} and lower bound N_{lower} are based on half the road width. The relative lateral positions n_{DS} and n_{US} determine whether to add an offset (second) term to shift one side of the boundary to the opposite side of the rectangular zone and form a passage with the other boundary. As illustrated in Figure 5(b), when the downstream car MC_{DS} drives on the right-hand side of the upstream car MC_{US}, the upper bound becomes the red dash line with the lower bound remaining as the blue dash line. These two dash lines together formulate a diamond-filled area that is passable. Vice versa, if the downstream car MC_{DS} is on the left-hand side of the upstream car, then the red and blue dot lines become active boundaries making the opposite diagonal area passable. The collision constraint is active only when the downstream car is within one car's length behind the upstream car. If the downstream car is further behind or has passed the abreast position, the constraint resumes functioning as normal road boundaries.

C. Cost function and constraints

In this study, the energy-saving scenario and overtaking scenario are formulated with different cost functions. In the energy-saving scenario, two major cases can be studied. The first one is to study the fastest lap time the downstream car can achieve with the existence of the upstream car wake. In this case, a classic minimal time maneuver (MTM) problem can be formulated with the cost function of:

$$J_{MTM} = \int_{s_0}^{s_t} (Sf + \epsilon \dot{u}^T W \dot{u}) ds \quad (35)$$

where Sf is the downstream car travel time for ds length along the track centerline and t_{US} is the lap time of the upstream car. The term $\epsilon \dot{u}^T W \dot{u}$ is a quadratic penalty term of the control derivatives which is added as regularization to the stage cost of the problem. W is a positive definite weight matrix, $\dot{u}$ and $\dot{u}^T$ denote the change rate of control vectors and their transposed form. In this paper, the controls include the change rates of steer angle δ, drive torque T_{drive} and brake torque T_{brake}. $\epsilon \in (10e-4, 10e-2)$ is a small value to minimize the compromise on lap time due to the penalty term. The function of this regularization term is to avoid singular arcs and oscillation in the solution caused by the nature of numerical algorithms [24] and to improve convergence performance [25].

In the same scenario, a second case can be formulated to study how much energy can be saved with slipstreaming while keeping a same pace as the upstream opponent car. For this purpose, the cost function will only contain the Lagrange stage cost which is

$$J_{ES} = \int_{s_0}^{s_t} (P_{drive} - P_{regen} + \epsilon \dot{u}^T W \dot{u}) ds \quad (36)$$

where s_0 and s_t are the initial and terminal length of the track respectively. To guarantee the downstream car keeps the same pace as the upstream car, an integral constraint needs to be applied as

$$\int_{s_0}^{s_t} Sf ds \leq t_{US} \quad (37)$$

where t_{US} is the lap time of the upstream car. It is worth noting that in this case where energy is being minimized, the lap time tends to be slower. As a result, despite equation (37) is formulated as an inequality integral constraint, the lap time would be naturally constrained to be the same as t_{US}. The result of two different problems in the energy-saving scenario will be presented in sector IV.

The overtaking scenario is also a classic MTM problem which shares the cost function of equation (35). In this scenario, for comparison, we formulate another problem to investigate what is the minimum power requirement to overtake without considering slipstreaming. The cost function only has a single term of the power limit to minimize:

$$J_{comp} = P_{limit} \quad (38)$$

where P_{limit} is the upper limit of drive power which has to be satisfied with a path constraint as $P_{drive} < P_{limit}$. For this special case, an additional integral boundary is introduced to guarantee an overtaking happens within the lap.

$$t_{DS} = \int_{s_0}^{s_t} Sf ds < t_{US} - t_{gap} \quad (39)$$

Where t_{DS} and t_{US} are the lap time of downstream and upstream cars respectively and t_{gap} is the initial time gap between the cars. It should be noted that in this way, a solver failing to generate a solution would suggest that overtaking under given constraints(e.g. big initial gap) is not possible.

Additionally, for all problems, we set the initial velocity of the downstream car the same as the upstream car.

$$u_{DS}(t_0) = u_{US}(0) \quad (40)$$

In general, for both problems, the system dynamics (e.g. equations 1-15) are included in $f(t, x(t), u(t), p)$, whereas the load transfer governing equations (16-19) are treated as equality path constraints included in $g(t, x(t), u(t), p)$. The bounds for states and controls, and path constraints of power limit and collision constraint are included in the inequality constraints $h(t, x(t), u(t), p)$. Finally, the integral constraints are treated as boundary constraints $g_b(x(t_0), x(t_f), u(t_0), u(t_f), p)$.

D. Scaling, smoothing and mesh refinement

The optimal control problem in this study is transcribed into a large non-linear programming problem (NLP) using the Legendre-Gauss-Radau (LGR) quadrature orthogonal collocation method and Radau's integration formula [26]. To implement this, the General-Purpose Optimal Control

MATLAB Toolbox GPOPS-II [27] and underlying interior point algorithm IPOPT [28] are used.

When using collocation method to solve an optimal control problem, the convergence performance of the solving can be significantly influenced by the scaling used in the problem formulation or transcription layer. In this study, we use a common method of scaling the base quantities into dimensionless quantities in order to improve the NLP solver performance. For instance, the vehicle mass of 900kg is scaled into a dimensionless value of 1. The car wheelbase of 3.1m is taken as the fundamental unit of length and given the dimensionless value of 1. In order to define the scaler for time variables, the gravitational acceleration g is scaled to the value of 1 so that the gravitational force of the car becomes a dimensionless value of 1. Using this method, other derived quantities such as the power of 200 kW now is 4.11, tyre normal force of 6000 N now is 0.68 and 50000 J of energy is scaled to 1.8, etc. This method will scale the NLP's variables in the original problem from a highly elongated hyperellipsoid into a more spherical space [24].

The interior point NLP algorithm assumes the constraint and object functions are continuously differentiable and it requires the first- and second-order derivative information. Therefore, the Heaviside step functions and if conditions in the collision constraints must be approximated in a smooth differentiable way. For this purpose, the Heaviside step function in the collision constraint is approximated using:

$$H(x) \approx H_s(x) = 0.5 + 0.5tanh\,(kx) \quad (40)$$

Similarly, the if condition can be described using the smoothed Heaviside step function $H_s(x)$. The collision boundaries of equations (33) and (34) become:

$$N_{upper} = 0.5w_{road} + (w_{car} + 0.5w_{road} - n_{DS})\big(H_s(s_{DS} - s_{US}) + H_s(s_{DS} - s_{US} + l_{car})\big)H_s(n_{DS} - n_{US}) \quad (35)$$

$$N_{lower} = 0.5w_{road} - (w_{car} + 0.5w_{road} + n_{DS})\big(H_s(s_{DS} - s_{US}) + H_s(s_{DS} - s_{US} + l_{car})\big)H_s(n_{US} - n_{DS}) \quad (36)$$

The accuracy of such approximation improves when the k value increases. To ensure that the approximation doesn't change the original problem significantly, $k \in (1e2, 1e4)$ is used in this paper.

In GPOPS-II, a large optimal control problem is segmented into mesh intervals and orthogonal collocation techniques are used in each mesh interval. The mesh refinement methods developed in the literature can be categorized into three categories, namely h method family which divides a mesh interval into multiple intervals, p method family where the order of approximation polynomials is increased and a hybrid of the two which is normally referred to as hp methods[29][30][31]. In this study, the method proposed by Liu et al. [32] is used. While other methods might end up with an unnecessarily dense mesh or high-order polynomial, this method is able to (1) reduce the degree of the polynomial when the high-order term in the power expansion is sufficiently small; and (2) merge adjacent mesh intervals when the degree of approximation intervals inside these intervals is essentially the same. This feature will ease the computational burden created by either dense initial mesh setup or over-refined meshes during the optimization iterations.

IV. Results and Discussion

In this section, the results of two different scenarios are presented. We also demonstrate how the trajectory of the slipstreaming car differs from that in the freestream and how the car's performance is affected due to slipstreaming. The layouts of the two tracks used are shown in figure 6.

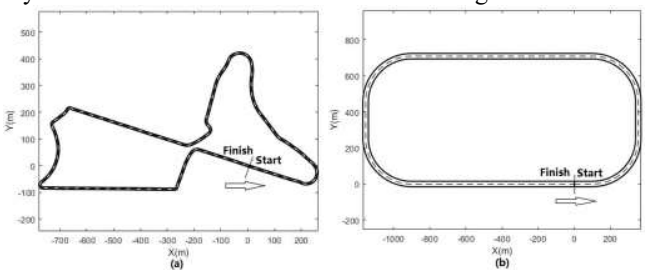


Fig. 6. Track layouts (a) Energy saving scenario; (b) Oval track overtaking scenario

A. Energy saving scenario

With the cost function of equation (35), we investigate how lap time can be improved given different upper limits of energy consumption and different initial time gaps between upstream and downstream cars. Figure 7(a) and (b) show the achievable lap times and improved time deltas.

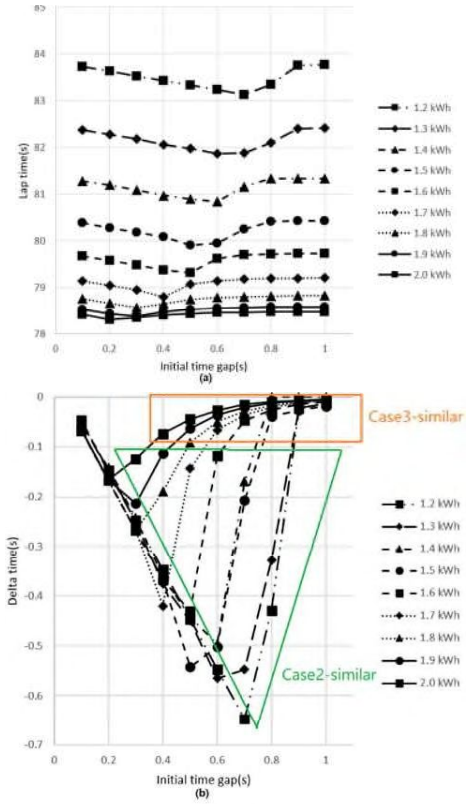


Fig. 7. Lap times and time deltas.

It should be noted that each line represents a series of cases where the lead car(i.e. reference car) and the downstream car have the same limit of energy consumption. It can be observed

that when the initial time gap is big (e.g 1s), there's hardly any improvement in lap time. As the initial gap reduces, the downstream car is able to perform a faster lap than the reference car. After a minimum point, the lap time starts to increase. This is because in such cases, the gap between the two cars is too small for the downstream car to further improve the lap time meanwhile stay behind the upstream car. To further improve the lap time, one has to consider overtaking. The feasibility and energy-optimal overtaking analysis has been presented in [33] and thus are not discussed here.

Another interesting feature that can be observed is that the biggest delta time under different energy constraints is different. The lap time can be improved more when less energy is allowed for both cars. Here we choose three representative cases (circled in figure 7) to demonstrate how different initial time gap affects the downstream car strategy. The presented three cases are all formulated under the energy constraint of 1.7kWh. As shown in figure 7(a), the case with a 0.4s initial time gap (later referred to as Case1) has the fastest lap time. With the gap increased to 0.5s the lap time (later referred to as Case2) improvement decreased and with the 0.6s gap (referred to as Case3) the performance recovered very closed to a freestream level.

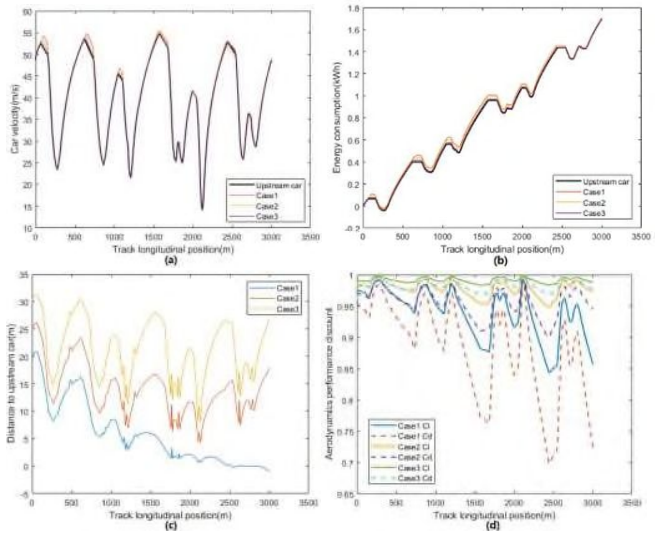


Fig. 8: Results from cases with 1.7kWh energy limit and initial time gaps of 0.4s, 0.5s and 0.6s. (a) Speed profiles; (b) Energy consumption; (c) Distance to the upstream car; (d) Aerodynamics performance discount

The first thing to notice is the difference in the speeds. All three cases share a similar early high-speed strategy. In the first half of the lap (before 1700m), the solutions suggest cars go higher speed than the upstream car in order to chase closer to it thus benefiting more discount in aerodynamics drag (shown in figure 8d). Note that figure 8d shows the value of $(1 - P_{loss}(\Delta t))$ in Equations (24) and (25). However, such an early high-speed strategy cost extra energy consumption as shown in figure 8b. To compensate for such energy costs, different solutions were found. For Case1, the strategy is to follow closely to the upstream car and the lower drag coefficient allows it to save enough energy to meet the 1.7kWh energy constraint by the end of the lap. In the other two cases, the downstream cars theoretically are able to chase the upstream car to a similar level as Case1. However, the solutions suggesting not doing so imply that this would cost too much energy for Case2 and Case3 in the early half. As a result, simply following the upstream car is no longer enough to make up for the extra energy consumption. A difference between Case2 and Case3 is the extent to which the downstream car chases the upstream car. In Case2 with a less initial gap, the downstream car deploys more energy to get closer to the upstream car. In the second half of the lap, the downstream car needs to back off a little driving at a slower speed than the reference car in order to save energy as shown in Figures 8a and 8b. It should be noted that although in Case2 the downstream car has to back off to meet the energy requirement, it still performs a lap quicker than the corresponding freestream case. It is very representative of the similar cases which are blocked in figure 7b. In contrast for Case3, with just 0.1s more gap than Case2, the initial gap becomes too large that the solution suggests chasing for temporary drag reduction is less worthy. Therefore, the chasing and backing off maneuvers are hardly observable in the figure. This Case3 also represents similar cases as blocked in figure 7b.

As previously mentioned, the lap time of the downstream car cannot be further improved when the initial gap is lower than a threshold (i.e. cases with 1.7kWh and 0.1-0.3s initial gap). However, in such cases, an alternative strategy is to save as much energy as possible instead of attempting overtaking which abandons the strategic advantage of slipstreaming. By using the cost function of eq.36, we investigate how energy can be saved by following and keeping the same pace with the upstream car. Four cases are presented in figure 9, namely Case4 (1.7kWh, 0.1s initial gap), Case5 (1.7kWh, 0.2s initial gap), Case6 (1.7kWh, 0.3s initial gap) and Case7 (1.7kWh, 0.5s initial gap).

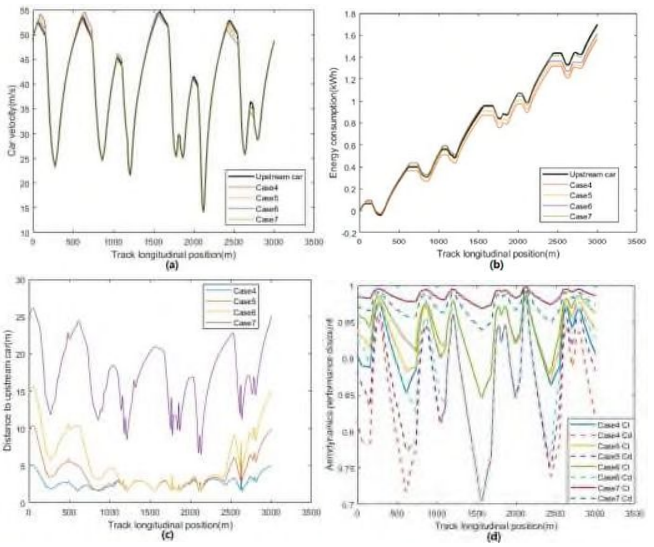


Fig. 9: Results from cases with 1.7kWh energy limit and initial

time gaps of 0.1s, 0.2s, 0.3s, 0.5s. (a) Speed profiles; (b) Energy consumption; (c) Distance to the upstream car; (d) Aerodynamics performance discount

Similarly, a chase-follow-backoff strategy can be observed. At the beginning of the lap, the downstream cars take a higher speed in order to get closer to the upstream car. Then in the middle sector of the lap (1200-2000m), Case4, Case5 and Case6 share the same strategy to follow closely the upstream car and benefit from a big drag coefficient discount. In the last sector, cars need to back off again to maintain the same overall pace as the upstream car. The result shows the downstream car can save 8%, 6.6% and 4.8% of energy consumption in Case4, Case5 and Case6 respectively.

Overall, a downstream car needs to chase harder and then back off more given a larger initial gap. However, when the initial gap is too big (e.g. Case7), the solution suggests that the downstream car can only benefit from a very limited amount of drag discount (only 1.4% of energy saved in Case7). The non-linearity in the result shows a potential in a multi-lap level strategy optimization that it is crucial to decide under what circumstances should the downstream car chase or follow the upstream car so that the slipstreaming is made the best of for a longer horizon. This raises a multi-stage decision-making problem featuring multiple players and thus is not discussed in this study.

B. Oval track overtaking scenario

In this scenario, we present a particular case with 0.2s of initial time gap due to two representative maneuvers observed.

Firstly, the overtaking in this case takes place near the end of the lap which is on the lower straight. The trajectory is shown in figure 10.

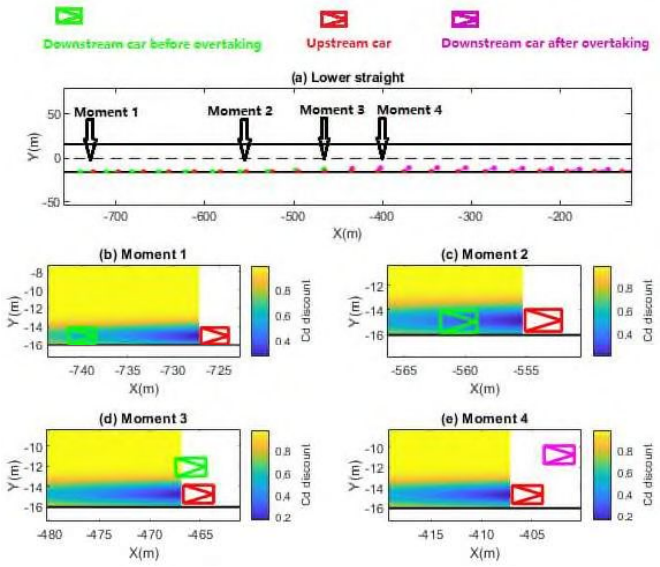


Fig. 10. Overtaking maneuver on the lower straight

After exiting the last corner, the downstream car stays in the wake of the upstream car. As aforementioned, two cars are driving under the same power limit. With the slipstreaming effect reducing the drag, the downstream car is able to gain a higher speed than the upstream car. After the downstream car gets enough speed advantage, it pulls out of the wake to execute the overtaking. This maneuver immediately brings higher drag and starts to slow down the downstream car. But with the momentum, it is able to move back to the normal racing line and then keep staying in the front of the upstream car. The speed profile and aerodynamics discount are shown in figure 11.

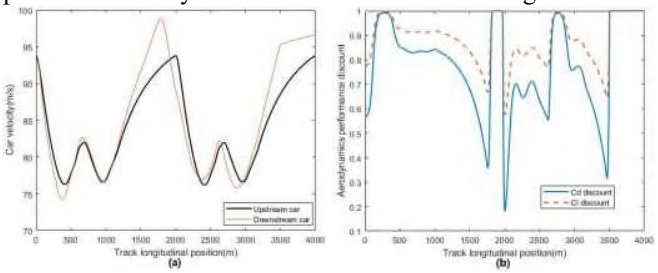


Fig. 11. (a) Speed profiles (b) Aerodynamics performance discount

It can be observed that the downstream car benefits from the drag discount hence its speed is much higher than the upstream car. After pulling out of the wake the acceleration of the downstream car is significantly reduced. Similarly, in the upper straight sector(1000-2000m), the slipstreaming effect can be observed. While the downstream car did not overtake in this sector, it can be observed that the aerodynamic discount rises back to 1 which suggests the car is out of the wake of the upstream car. This behaviour is detailed in figure 12 below as another representative maneuver.

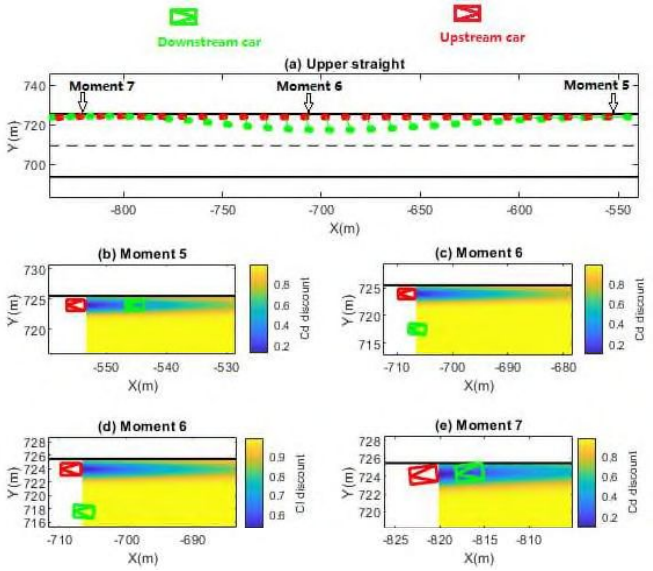


Fig. 12. Slipstreaming trajectory on the upper straight

Up until moment 5, the downstream car has been staying within the wake in order to chase the upstream car. When approaching the end of the straight to enter the following corner, the solution suggests an out-of-wake trajectory for the downstream car. The cause of such a solution is the demand for braking performance because the downstream car is at a much higher speed and needs to slow down harder to an appropriate speed for the upcoming corner. Pulling out of the wake helps in two aspects. Firstly, the drag is much higher outside the wake (figure 12c). At such high speed, this aerodynamic drag contributes a significant part of

the total brake force. Secondly, the downstream car suffers less downforce deficit outside the wake (figure 12d). This higher downforce (discount close to 1) helps guarantee the mechanical brake force generated from the tyres. Therefore, the joint effect of drag and downforce outside the wake allows the downstream car to slow down effectively while maintaining a close distance from the upstream car to preserve a chance for later overtaking. It should be noted that the downstream car performance is also affected due to the downforce discount. As a result, it can be observed in the G-G plot in Figure 13 that the maximum lateral acceleration of the downstream car is slightly lower than the upstream car. An additional interesting feature of the solution trajectory can be observed in the last corner of the lap. The downstream car opted for a slightly different line compared to the upstream car. The reasons are assumed to be (1) this deviation allows the downstream car to suffer less downforce deficit and maintain a competitive speed in the corner and (2) this alternative racing line gives the downstream car a better corner exiting speed (can be observed in Figure 11a at around 3000m) which benefit overtaking later in the straight.

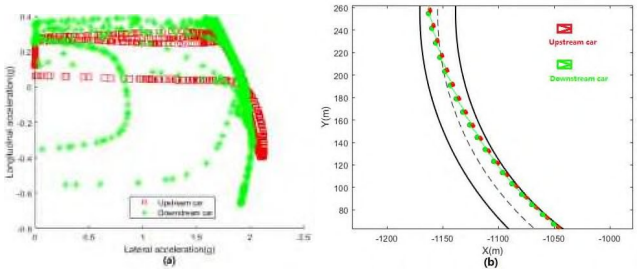


Fig. 13. (a) G-G plot (b) Trajectory in the last corner

The results demonstrated above are computed using cost function e.q. 35 and the downstream car is under the same power limit of 500kW as the upstream car. If the slipstreaming effect is ignored and attempt overtaking by adding more power to the car, the minimum power required is 526kW solved by using the cost function e.q. 38. In this case, the overtaking is achieved purely by deploying more power on the straight and the solution trajectory has few interesting features and thus is not shown here.

V. Conclusion

In this paper, we proposed a new approach to model the slipstreaming effect based on published data. This new approach enables investigations of the optimal performance or strategy of a downstream car in lap time simulation. With this technique, two different scenarios are studied. The first one is to study how energy can be saved by accounting for the slipstreaming effect in an electric racing series. The second is to study how to make the best of the upstream car's wake to overtake.

In the energy-saving scenario, it is obvious that to benefit from slipstreaming, the downstream car needs to get close to the upstream car. However, it is shown from the result that the worthiness of such a strategy varies depending on the initial gap. If the initial gap is relatively big, the amount of energy that potentially can be saved in slipstreaming is not enough to make up for the extra energy consumption in the early chasing. In such cases, a back-off maneuver is needed near the end of a lap in order to meet the boundary constraint (e.g. pace or energy consumption). If the initial gap further increases, it becomes less effective to pursue the slipstreaming benefit. It is noteworthy to highlight that in the single-lap scenario investigated within this study, the back-off strategy emerges as the most optimal solution. Nevertheless, in scenarios involving multiple laps and cars, such an approach may exhibit less efficiency. The findings presented in this paper lay a solid groundwork at the individual lap level, which can serve as a basis for formulating strategies at the multi-lap or race level.

In the oval track scenario, due to high overall speed, both aerodynamic drag and downforce in the wake affect the downstream car trajectory. The result shows that the reduction in drag benefits the downstream in gaining straight-line speed. However, the solution suggests that the downstream car needs to drive outside the wake to preserve braking performance before entering a corner. Additionally, when driving through a corner, an alternative racing line is also preferable because the lower downforce in the wake would affect the downstream car's lateral performance.

Overall, this paper presents a novel way to model the slipstreaming effect and how it affects the energy management and overtaking strategies respectively in two different scenarios. This approach can potentially aid designs in highly aerodynamic-sensitive vehicles.

Appendix

A. Tyre model

.

The tyre model used in this paper is an empirical tyre model with linearized interpolation for peak values of longitudinal and lateral friction coefficients. The longitudinal and lateral forces are given by:

$$F_{xi} = \mu_{xi} F_{zi} \frac{\kappa_{ni}}{\sqrt{\alpha_{ni}^2 + \kappa_{ni}^2 + \epsilon}} \quad \text{(A1)}$$

$$F_{yi} = \mu_{yi} F_{zi} \frac{\alpha_{ni}}{\sqrt{\alpha_{ni}^2 + \kappa_{ni}^2 + \epsilon}} \quad \text{(A2)}$$

where F_{zi} is the tyre normal force, κ_{ni} and α_{ni} are the normalized tyre slip with respect to the slip value where peak friction coefficient happens:

$$\alpha_{ni} = \frac{\alpha_i}{\alpha_{maxi}} \quad \text{(A3)}$$

$$\kappa_{ni} = \frac{\kappa_i}{\kappa_{maxi}} \quad \text{(A4)}$$

The slip angles α_{ni} and ratios κ_{ni} are given by:

$$\alpha_1 = \delta - \arctan\left(\frac{v+\omega a}{u-\omega w}\right), \kappa_1 = -1 + \frac{R\omega_1}{cos\delta(u-\omega w) - sin\delta(v+\omega a)} \quad \text{(A5)}$$

$$\alpha_2 = \delta - \arctan\left(\frac{v+\omega a}{u+\omega w}\right), \kappa_2 = -1 + \frac{R\omega_2}{cos\delta(u+\omega w) - sin\delta(v+\omega a)} \quad \text{(A6)}$$

$$\alpha_3 = -\arctan\left(\frac{v-\omega b}{u+\omega w}\right), \kappa_3 = -1 + \frac{R\omega_3}{u+\omega w} \quad \text{(A7)}$$

$$\alpha_4 = -\arctan\left(\frac{v-\omega b}{u-\omega w}\right),\ \kappa_4 = -1 + \frac{R\omega_4}{u-\omega w} \quad \text{(A8)}$$

In which ω_i is the angular velocity of each wheel and R the tyre radius.

The peak friction values are given by linear interpolation which treats them as linear functions or the tyre normal loads. The symbols are explained in table A1.

$$\mu_{x\,max} = (F_z - F_{z\,R1})\left(\frac{\mu_{x\,max2}-\mu_{x\,max1}}{F_{z\,R2}-F_{z\,R1}}\right) + \mu_{x\,max1} \quad \text{(A9)}$$

$$\mu_{y\,max} = (F_z - F_{z\,R1})\left(\frac{\mu_{y\,max2}-\mu_{y\,max1}}{F_{z\,R2}-F_{z\,R1}}\right) + \mu_{y\,max1} \quad \text{(A10)}$$

$$\kappa_{max} = (F_z - F_{z\,R1})\left(\frac{\kappa_{max2}-\kappa_{max1}}{F_{z\,R2}-F_{z\,R1}}\right) + \kappa_{max1} \quad \text{(A11)}$$

$$\alpha_{max} = (F_z - F_{z\,R1})\left(\frac{\alpha_{max2}-\alpha_{max1}}{F_{z\,R2}-F_{z\,R1}}\right) + \alpha_{max1} \quad \text{(A12)}$$

TABLE A1
Description of symbols

Symbol	Description	Front value	Rear value
$F_{z\,R1}$	Reference normal load 1	2000 N	2000 N
$F_{z\,R2}$	Reference normal load 2	6000 N	6000 N
$\mu_{x\,max1}$	Peak longitudinal friction coefficient at load 1	1.4	1.75
$\mu_{x\,max2}$	Peak longitudinal friction coefficient at load 2	1.12	1.4
κ_{max1}	Slip coefficient for the friction peak at load 1	0.11	0.11
κ_{max2}	Slip coefficient for the friction peak at load 2	0.10	0.10
$\mu_{y\,max1}$	Peak lateral friction coefficient at load 1	1.62	1.8
$\mu_{y\,max2}$	Peak lateral friction coefficient at load 2	1.3	1.45
α_{max1}	Slip angle for the friction peak at load 1	9°	9°
α_{max2}	Slip angle for the friction peak at load 2	8°	8°
Q_x	Longitudinal shape factor	1.9	1.9
Q_y	Lateral shape factor	1.9	1.9

Next, the longitudinal and lateral friction coefficients in equations (13) and (14) are described by

$$\mu_{xi} = \mu_{xi\,max}\sin\left(Q_x \arctan\left(\frac{\pi}{2\arctan(Q_x)}\sqrt{\alpha_{ni}^2+\kappa_{ni}^2}\right)\right) \quad \text{(A13)}$$

$$\mu_{yi} = \mu_{yi\,max}\sin\left(Q_y \arctan\left(\frac{\pi}{2\arctan(Q_y)}\sqrt{\alpha_{ni}^2+\kappa_{ni}^2}\right)\right) \quad \text{(A14)}$$

where $Q_x$and Q_y Are shaping factors.

B. Computational information

TABLE B1
Computer spec, solver and time

CPU	i7 6700HQ
Linear solver	ma57
Transcription toolbox	GPOPS
Nonlinear program solver	IPOPT 3.12.3
Differentiation toolbox	ADiGator
Average solve time	40 mins

It should be noted that the solve time depends on multiple factors including not only the hardware but also how efficient the other components are. In this study, we used ADiGator to generate the Jacobian and Hessian which cost a fair amount of time. Such information can be calculated analytically and potentially more efficiently. Also, the ma57 solver wasn't the faster linear solver that IPOPT supports. Therefore, there is still a big potential to shorten the solve time.

Authors provided the average solve time here because the two categories of studies in this paper performed differently in solve time. The ones where the downstream car only did slipstreaming in the entire lap solved relatively quicker. Whereas when overtaking happens, it solved slower. Authors believe this is due to the collision constraint and the smoothing factor k in equation (40). This can be tuned to make the Heaviside step function H(x) approximation smoother which is expected to improve the convergence but the downside of this is that the description of the collision zone would become less accurate. The cases studied in this paper all solved. If one wants to formulate a force-overtake problem, it potentially can fail due to feasibility issue. However this is not investigated in this paper.

C. Aero performance discount parameters

TABLE C1
Aero performance discount parameters

Parameter	Value
ξ_{Cd}	0.00011
ξ_{Cl}	0.000057
σ_{Cd}	1.6
σ_{Cl}	1.6
γ_C	1.273
k_C	5

$$\xi_C u_{US}^2 e^{\frac{-\Delta n^2}{\sigma_C}}$$

REFERENCES

[1] Ritzmann, Johannes, et al. Fuel-optimal power split and gear selection strategies for a hybrid electric vehicle. No. 2019-24-0205. SAE Technical Paper, 2019.

[2] Elbert, Philipp, et al. "Engine on/off control for the energy management of a serial hybrid electric bus via convex optimization." IEEE Transactions on Vehicular Technology 63.8 (2014): 3549-3559.

[3] Tremlett, Anthony J., et al. "Optimal control of motorsport differentials." Vehicle System Dynamics 53.12 (2015): 1772-1794.

[4] Perantoni, Giacomo, and David JN Limebeer. "Optimal control for a formula one car with variable parameters." Vehicle System Dynamics 52.5 (2014): 653-678.

[5] Tremlett, A. J., and D. J. N. Limebeer. "Optimal tyre usage for a formula one car." Vehicle System Dynamics 54.10 (2016): 1448-1473.

[6] Limebeer, David JN, Giacomo Perantoni, and Anil V. Rao. "Optimal control of formula one car energy recovery systems." International Journal of Control 87.10 (2014): 2065-2080.
[7] Ebbesen, Soren, et al. "Time-optimal control strategies for a hybrid electric race car." IEEE Transactions on control systems technology 26.1 (2017): 233-247.
[8] Herrmann, Thomas, et al. "Energy management strategy for an autonomous electric racecar using optimal control." 2019 IEEE Intelligent Transportation Systems Conference (ITSC). IEEE, 2019.
[9] Liu, Xuze, Abbas Fotouhi, and Daniel J. Auger. "Optimal energy management for formula-E cars with regulatory limits and thermal constraints." Applied Energy 279 (2020): 115805.
[10] Liu, Xuze, and Abbas Fotouhi. "Formula-E race strategy development using artificial neural networks and Monte Carlo tree search." Neural Computing and Applications (2020): 1-17.
[11] Perantoni, Giacomo, and David JN Limebeer. "Optimal control of a formula one car on a three-dimensional track—Part 1: Track modeling and identification." Journal of Dynamic Systems, Measurement, and Control 137.5 (2015).
[12] Limebeer, David JN, and G. Perantoni. "Optimal control of a formula one car on a three-dimensional track—Part 2: Optimal control." Journal of Dynamic Systems, Measurement, and Control 137.5 (2015).
[13] Masouleh, Mehdi Imani, and David JN Limebeer. "Optimizing the aero-suspension interactions in a formula one car." IEEE Transactions on Control Systems Technology 24.3 (2015): 912-927.
[14] Wilson, Michael R., Robert G. Dominy, and Adam Straker. "The aerodynamic characteristics of a race car wing operating in a wake." SAE International Journal of Passenger Cars-Mechanical Systems 1.2008-01-0658 (2008): 552-559.
[15] Soso, M. D., and P. A. Wilson. "Aerodynamics of a wing in ground effect in generic racing car wake flows." Proceedings of the Institution of Mechanical Engineers, Part D: Journal of Automobile Engineering 220.1 (2006): 1-13.
[16] Gan, Edwin Chern Junn, Mikhail Fong, and Yee Luon Ng. "CFD Analysis of Slipstreaming and Side Drafting Techniques Concerning Aerodynamic Drag in NASCAR Racing."
[17] Newbon, Joshua, David Sims-Williams, and Robert Dominy. "Aerodynamic analysis of Grand Prix cars operating in wake flows." SAE International journal of passenger cars. Mechanical systems. 10.1 (2017): 318-329.
[18] Guerrero, Alex, and Robert Castilla. "Aerodynamic Study of the Wake Effects on a Formula 1 Car." Energies 13.19 (2020): 5183.
[19] Pacejka, Hans. Tire and vehicle dynamics. Elsevier, 2005.
[20] Kelly, Daniel Patrick. "Lap time simulation with transient vehicle and tyre dynamics." (2008).
[21] Viana, Ícaro Bezerra, Hussain Kanchwala, and Nabil Aouf. "Cooperative Trajectory Planning for Autonomous Driving Using Nonlinear Model Predictive Control." 2019 IEEE International Conference on Connected Vehicles and Expo (ICCVE). IEEE, 2019.
[22] You, Feng, et al. "Trajectory planning and tracking control for autonomous lane change maneuver based on the cooperative vehicle infrastructure system." Expert Systems with Applications 42.14 (2015): 5932-5946.
[23] Hayashi, Ryuzo, et al. "Autonomous collision avoidance system by combined control of steering and braking using geometrically optimised vehicular trajectory." Vehicle system dynamics 50.sup1 (2012): 151-168.
[24] Masouleh, Mehdi Imani. Optimal control and stability of four-wheeled vehicles. Diss. University of Oxford, 2017.
[25] Schwartz, Adam Lowell. Theory and implementation of numerical methods based on Runge-Kutta integration for solving optimal control problems. Diss. University of California, Berkeley, 1996.
[26] Davis, Philip J., and Philip Rabinowitz. Methods of numerical integration. Courier Corporation, 2007.
[27] Patterson, Michael A., and Anil V. Rao. "GPOPS-II: A MATLAB software for solving multiple-phase optimal control problems using hp-adaptive Gaussian quadrature collocation methods and sparse nonlinear programming." ACM Transactions on Mathematical Software (TOMS) 41.1 (2014): 1-37..
[28] Wächter, Andreas, and Lorenz T. Biegler. "On the implementation of an interior-point filter line-search algorithm for large-scale nonlinear programming." Mathematical programming 106.1 (2006): 25-57.
[29] Patterson, Michael A., William W. Hager, and Anil V. Rao. "A ph mesh refinement method for optimal control." Optimal Control Applications and Methods 36.4 (2015): 398-421.
[30] Darby, Christopher L., William W. Hager, and Anil V. Rao. "Direct trajectory optimization using a variable low-order adaptive pseudospectral method." Journal of Spacecraft and Rockets 48.3 (2011): 433-445.
[31] Darby, Christopher L., William W. Hager, and Anil V. Rao. "An hp-adaptive pseudospectral method for solving optimal control problems." Optimal Control Applications and Methods 32.4 (2011): 476-502.
[32] Liu, Fengjin, William W. Hager, and Anil V. Rao. "Adaptive mesh refinement method for optimal control using nonsmoothness detection and mesh size reduction." Journal of the Franklin Institute 352.10 (2015): 4081-4106.
[33] Liu, Xuze, Abbas Fotouhi, and Daniel J. Auger. "Energy-optimal overtaking maneuvers of Formula-E cars." Vehicle System Dynamics (2022): 1-28.



Dr Xuze Liu received his BSc and MEng degrees from Beijing Institute of Technology (BIT), Beijing, China, in 2015 and 2017 respectively and received his MSc from Cranfield University, UK in 2018. He completed this Ph.D. degree within Advanced Vehicle Engineering Centre, School of Aerospace, Transport and Manufacturing, Cranfield University in 2022.



Dr Abbas Fotouhi (M'13–SM'21) is Senior Lecturer in Advanced Vehicle Engineering Centre at Cranfield University. He has more than fifteen years research experience in systems modelling, simulation, optimization, and control. He has also extensive practical and algorithmic experience of applying Artificial Intelligence and Machine Learning techniques in engineering problems. His current research is focused on vehicular systems including hybrid and electric vehicle powertrain systems, energy storage technologies and autonomous cars.



Dr Marco Cecotti received the PhD degree in electrical engineering from Oxford Brookes University, UK, in 2013. He worked for Tata Motors and Dyson on different automotive projects, focused on the control of electric and hybrid electric powertrains, and the development of autonomous vehicles. He then moved to Cranfield University to work on several research projects focused on vehicle automation. Dr Cecotti is now a Lecturer at the Advanced Vehicle Engineering Centre at Cranfield University, UK. His research interests include vehicle trajectory control, path planning, localisation and sensor fusion, applied to autonomous ground vehicles.



Dr Daniel Auger is Professor in Electrification, Automation and Control in Cranfield University's Advanced Vehicle Engineering Centre. He is an expert in control systems, vehicle electrification and autonomy. He leads major work streams on self-driving cars, and he has pioneered advanced battery management algorithms for lightweight lithium-sulfur batteries. He has also introduced new state-of-the-art MSc teaching in applied control engineering and launched a new course in connected and autonomous vehicle engineering.



https://dspace.org/

Optimal control of race car with aerodynamic slipstreaming effect

Liu, Xuze; Fotouhi, Abbas; Cecotti, Marco; Auger, Daniel

2024-11-01
Institute of Electrical and Electronics Engineers (IEEE)
https://doi.org/10.1109/TCST.2024.3395722
Liu X, Fotouhi A, Cecotti M, Auger D. (2024) Optimal control of race car with aerodynamic slipstreaming effect. IEEE Transactions on Control Systems Technology. Volume 32, Issue 6, November 2024, pp. 2136-2148

Downloaded from a DSpace repository. https://dspace.org/